[1] Department of Physics, University of Jaén, Spain
[2] Department of Applied Physics, University of Almería, Spain
[3] Department of Computer Sciences, University of Jaén, Spain

Proposal of a function for modelling the hourly frequency distributions of photosynthetically active radiation

J. Tovar-Pescador[1], **D. Pozo-Vazquez**[1], **J. Batlles**[2], **G. López**[2], and **D. Muñoz-Vicente**[3]

With 4 Figures

Summary

Solar irradiance is a key factor in the physiological processes of living beings. To obtain simple correlations for the estimation of the performance of biological systems, which transform the solar energy by photosynthesis, and to generate synthetic data, it is necessary to know the frequency distributions of photosynthetically active radiation (PAR). In this work we carried out an analysis of the properties of hourly values of PAR data, using 9 years of data collected in southern Spain. In particularly, its dependence on the optical mass, for all type of skies including cloudy skies, is studied. Results shows that, for a given value of the optical mass, the PAR density distributions are not symmetrical and have a certain degree of bimodality. The increment in the optical mass value has two effects on the PAR distributions, the first one is a shift toward lower values of the maximum and the second one is a decrease in the range of PAR values. Finally, a model of the frequency distribution of PAR values, based on a new kind of functions related to the Boltzmann's statistic, is proposed. The parameters of these functions depend just on the optical mass. Results show a very good agreement between the data and the model proposed.

1. Introduction

The knowledge of statistical properties of solar radiation is of interest for several reasons; one is the purely meteorological interest, toward the understanding of how nature behaves; the second one is the usefulness that these properties have in modelling systems in which solar radiation is an important input parameter; finally, the knowledge of the statistical properties is important to obtain synthetic data for simulating the solar radiation. Solar radiation supports life by modifying temperature and providing the energy required in many natural process, such as photosynthesis. Particularly, the waveband and energy content of solar radiation acts as a constraint on the evolution of photobiological processes. The spectral band 400–700 nm is named Photosynthetically Active Radiation (PAR) and is responsible for the photosynthesis process. The knowledge of PAR, therefore, is necessary in different applications related to the biochemical process of photosynthesis, the physiology of the plants and the biomass production. PAR is the general term that covers both photon and energy terms. Photosynthetic photon flux density, Q_p, is the global PAR density flux defined as the photon flux density (1 μmol photons m^{-2} s^{-1} = 6.022×10^{17} photons m^{-2} s^{-1} = μE m^{-2} s^{-1}). This is the number of

photons in the 400–700 nm waveband incidents per unit time on a unit surface.

The literature includes many works that deal with the statistical properties of broadband solar radiation (Bendt et al., 1981; Suehrcke et al., 1988; Feuillard et al., 1989; Gordon et al., 1989; Skarveit et al., 1992; Aguiar et al., 1992; Olseth et al., 1993; Gansler et al., 1995; Jurado et al., 1995; Tovar et al., 1998), but the analysis of other spectral ranges, such as PAR, are less abundant, probably due to the still scarce PAR data measured around the world.

Some works have dealt with the statistical treatment of PAR variability (Ross, 1999) but there is shortage of works dealing with the statistical time features of PAR data.

The aim of this work is to increase the current knowledge of the PAR statistical properties, including its dependence on the optical air mass. We use cumulative distribution functions and density functions, to characterize these statistical properties and the dependence on the optical mass. This paper is organized as follows. The first part of Section 2 describes the data used. In particular, the climatic aspects of the two locations where data were collected are discussed. The second part of Section 2 describes the statistical analysis procedures carried out in this work. Section 3 shows the results of the analysis. In the first part of Section 3, a study of the dependence of PAR on the optical mass is carried out. In the second part, the observed behavior is modelled. Finally, some conclusions of the results are given in Section 4.

2. Experimental data and method of analysis

The data used in this study were recorded in the radiometric stations of the University of Almería (36.83° N, 2.41° W, 20 m a.m.s.l.) and in the radiometric station of Armilla (37.18° N, 3.58° W, 660 m a.m.s.l.) both in southern Spain. Almería is a coastal site characterised by a moderate climate with scarce rainfall. The radiometric station of Armilla was installed by the University of Granada and the Spanish National Meteorological Institute in a little town located near Granada (Spain), characterised by cool winters and hot summers. The diurnal temperature range is rather wide with the possibility of freez-

ing on winter nights. Most rainfall occurs in spring and winter. The summer is very dry, with little rainfall in July and August. At Almería, the data were collected from 1991 to 1999 and in Armilla from January 1993 to December 1996. In the two stations the radiometer used to measure the photosynthetic radiation active photon flux density was a LICOR model 190 SA quantum sensor. Another quantum sensor was equipped with a polar axis shadowband in order to measure the diffuse photosynthetic active photon flux density incident on a horizontal surface. The data set includes other meteorological variables, such as global and diffuse broadband solar radiation, registered using Kipp and Zonen CM-11 pyrometers, ambient air temperature, relative humidity and other radiometric and meteorological variables not used in the present study. The drift of the calibration constants of the quantum sensors have been evaluated both by means of a calibrated standard lamp and by field comparison with measurements performed by a well-calibrated field spectroradiometer (LI-1800). The datalogger was programmed to 5 s sampling rate and 1 min average in Armilla and 10 min average in Almería. Measurements of solar global irradiance have an estimated experimental error of about 2–3%, while the quantum sensor has a relative error of less than 5%. The periods covered by the data set guarantees a complete range of seasonal conditions and solar angles among the samples taken. To avoid cosine response errors, we have used only data corresponding to solar zenith angle less than 85°.

We have divided the data set into two randomly obtained sub-data sets of hourly data. The first one includes two thirds of the total data, and we have used it for analysing and modelling the PAR. We have used the rest of the data set (one third of the total data) for testing purposes. The analysis of PAR values has been carried out characterizing the cumulative distribution function $F(Q_p, t)$:

$$F(Q_p, t) = P[Q_p(t) \leq Q_p] \qquad (1)$$

This function represents the probability that the event $Q_p(t)$ at time t is smaller than the given value Q_p. This quantity also represents the fraction of time during which the variable is below a given value. We have divided the possible range (0–2000 μE m^{-2} s^{-1} in our case) of Q_p into 50

intervals, each $40\,\mu\mathrm{E}\,\mathrm{m}^{-2}\,\mathrm{s}^{-1}$ in width. The distributions can be also characterized by the density function $f(Q_p, t)$, given by:

$$f(Q_p) = \frac{\partial F(Q_p)}{\partial Q_p}, \qquad (2)$$

omitting the t dependence for more clarity, with the normalization condition:

$$\int_0^{Q_{p,max}} f(Q_p)dQ_p = 1. \qquad (3)$$

The functions included in the definition depend on the optical air mass. Consequently, we have analyzed the probability density distribution and the cumulative distributions functions of Q_p conditioned to particular values of optical air mass denoted, respectively, $f(Q_p|m_a)$ and $F(Q_p|m_a)$. In order to fit the functions, we used the minimum-square method through an iterative process that uses the Levenberg-Marquardt procedure. We have imposed the constraint given by Eq. 10.

3. Results and discussion

3.1 Dependence of radiative values on the optical air mass

The solar radiation received at the earth surface depends mainly on its value at the top of the atmosphere, the optical air mass and the atmospheric conditions. The optical air mass depends on the sun position relative to the considered place. In a Rayleigh atmosphere, the first two variables provide the maximum possible radiative value disposable at the earth surface, after the depletion caused by the scattering and absorption effects. The optical air mass depends on zenith angle, θ_z, according to Kasten (1966) equation:

$$m_r = [\cos\theta_z + 0.15(93.885 - \theta_z)^{-1.253}]^{-1}. \qquad (4)$$

This equation is valid for a standard pressure of 1013.25 hPa at sea level; for other pressures, it should be modified. Although this task is complex, the equation $m_a = m_r(p/1013.25)$, where p is local pressure in hPa, is commonly employed to obtain the relative optical air mass for local conditions. The pressure above sea level may be obtained from $p = p_0 \exp(-0.0001184\ z)$, where z is the station altitude, in meters above sea level (Iqbal, 1983).

Figure 1 shows the dependence of the PAR on the optical mass. Plotted values correspond to the whole data set. For a given value of optical air mass, there is a wide range of PAR values, from 0 to a maximum value, different for every optical air mass value. When the optical mass increases, and given that the attenuation is proportional to the atmospheric mass, the incident radiation at earth surface, Q_p decreases. There are different
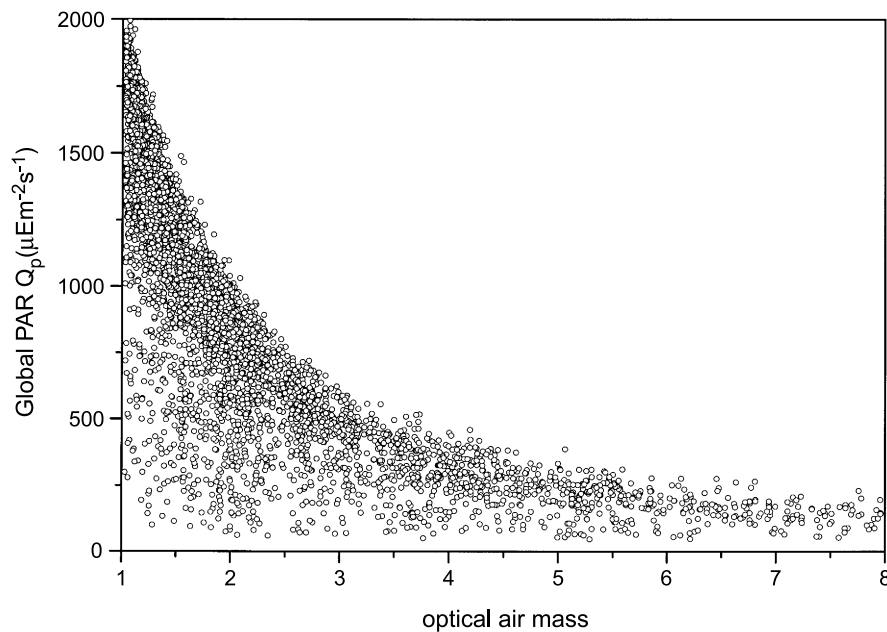
Fig. 1. Representation of global PAR versus optical air mass values. Only 8000 randomized points are represented for more clarity

Q_p values for a given optical mass, a consequence of the availability of several sky conditions for every optical air mass. Let us consider a narrow interval of optical air mass. The points on the top correspond to clear sky conditions, that is, a Rayleigh atmosphere. The lower values correspond to other sky conditions. The different point density is due to the different probability of every atmospheric condition. The bottom zone corresponds to cloudy sky conditions, where the radiative fluxes are very small. The highest Q_p values are given by continuous upper boundary in Fig. 1. Above this boundary, some values appear due to the enhancement of radiation values by multiple reflections of light on the clouds. Note the great density of values near the maximum.

3.2 Frequency distributions of PAR hourly values conditioned to the optical air mass

To analyze the frequency distribution of PAR data, we have firstly selected the PAR values for a given optical air mass value, following similar criteria to other studies (Suehrcke et al., 1988; Skartveit et al., 1992; Tovar et al., 1998). Table 1 shows, for the first data set (used to develop the model), the selected optical air mass intervals and the relevant statistical information of these intervals. Table 2 shows the same infor-

mation for the second data set, used for testing purposes. For every category, we present the number of experimental cases, the mean and the maximum values of PAR and the standard deviation. The values are smaller than $2000\,\mu E\,m^{-2}\,s^{-1}$ for any optical air mass.

Figure 2 shows the distribution density functions obtained, $f(Q_p|m_a)$, based on the first data set for every optical air mass. For a better comparison, we have considered $2000\,\mu E\,m^{-2}\,s^{-1}$ as the maximum possible value of PAR in all the distributions and we have obtained the normalized histograms using 50 partitions, $40\,\mu E\,m^{-2}\,s^{-1}$ in width.

The density distributions are not symmetrical and show a certain degree of bimodality. Furthermore, note the lower probability for low rather than for high PAR values. Two zones in the distributions can be delimited: the first one centered around the maximum value, the other one at the left of the maximum value and corresponding to lower PAR values.

Note that an increment in the optical mass value leads to a shift to the left of the maximum value, that is, an increment of the probability of lower values. Note also that the range of variation of the PAR values considerably diminishes when the optical mass increases. For optical mass value 1, Q_p values between 0 and $2000\,\mu E\,m^{-2}\,s^{-1}$ can be found, while for optical

Table 1. Statistics of the data set used to obtain the model. Values have been computed for each optical air mass interval

Interval	Assigned nominal value	Number of hours	Average of Q_p	Standard deviation ($\mu E\,m^{-2}\,s^{-1}$)	Maximum value of PAR ($\mu E\,m^{-2}\,s^{-1}$)
$1.0 < m_a < 1.2$	$m_a = 1.0$	5201	1499.7	326.02	1724.5
$1.4 < m_a < 1.6$	$m_a = 1.5$	4030	1034.8	271.25	1236.8
$1.8 < m_a < 2.2$	$m_a = 2.0$	4159	707.85	222.1	1074.2
$2.3 < m_a < 2.7$	$m_a = 2.5$	2163	529.36	170.1	817.7
$2.75 < m_a < 3.25$	$m_a = 3.0$	2468	381.1	141.36	491.2

Table 2. Statistics of the data set reserved for testing purposes. Values have been computed for each optical air mass interval

Interval	Assigned nominal value	Number of hours	Average of Q_p	Standard deviation ($\mu E\,m^{-2}\,s^{-1}$)	Maximum value of PAR ($\mu E\,m^{-2}\,s^{-1}$)
$1.0 < m_a < 1.2$	$m_a = 1.0$	2642	1492.7	327.75	1984.5
$1.4 < m_a < 1.6$	$m_a = 1.5$	2102	998.3	269.58	1674.6
$1.8 < m_a < 2.2$	$m_a = 2.0$	1824	702.98	238.11	1231.3
$2.3 < m_a < 2.7$	$m_a = 2.5$	1474	532.03	158.27	952.3
$2.75 < m_a < 3.25$	$m_a = 3.0$	1233	390.33	143.22	892.1
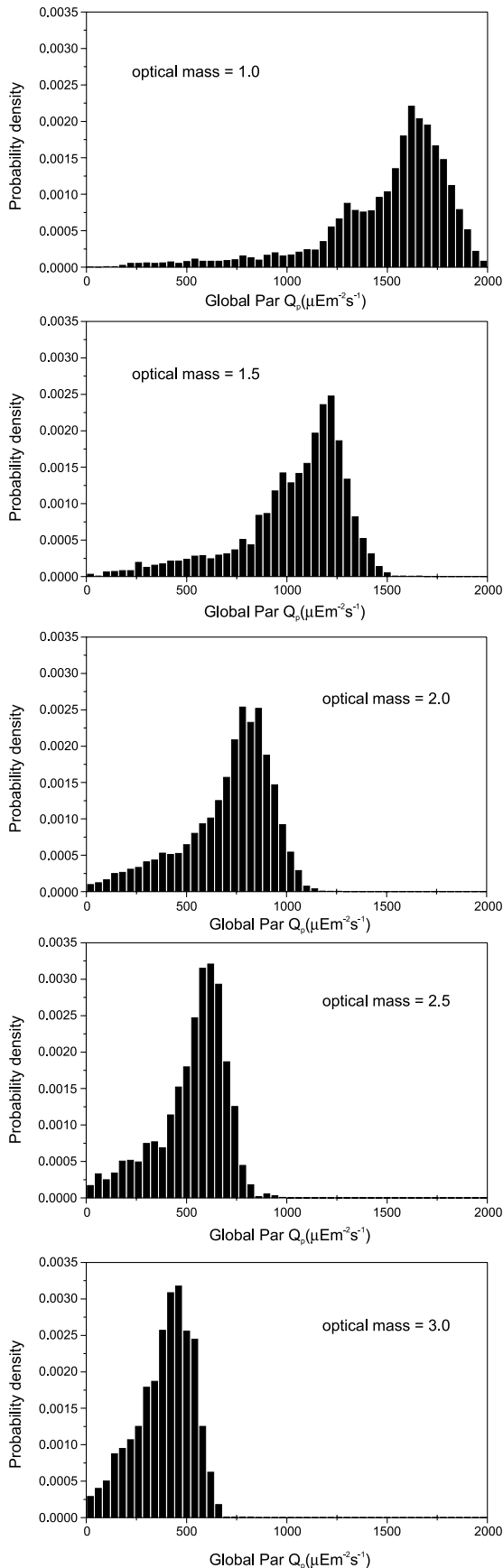
mass 3, the range is reduced to the interval 0 to $700\,\mu E\,m^{-2}\,s^{-1}$. This is due to the fact that an increment in the optical air mass implies a greater depletion of the solar radiation. An additional effect is produced by the hiding of the sun by the clouds, more evident for high zenith angles (Tovar et al., 1998; Suehrcke et al., 1988).

To obtain a model of the statistical behavior of solar radiation, we have hypothesized that the different PAR values probabilities, for a given optical mass, are due to two contributions. The first is associated with cloudless conditions, providing high Q_p values. The other one is associated with, fundamentally, cloudy conditions and provides low Q_p values. This second can be also associated with other atmospheric conditions having great optical masses (low sun elevation angles). High PAR values in the distribution, on the right of the density function, always correspond to clear skies. Low PAR values, on the left of the distribution, correspond fundamentally to cloudy skies. The probability of a particular PAR value is related to the sum of the probabilities of the two situations described.

The decrease of the Q_p range when the optical mass increases can be related to several factors. Given that the PAR radiation cannot have greater values than those corresponding to the Rayleigh atmosphere, the increment in the optical mass implies a diminution of the maximum PAR values. As consequence, the values move to the left of the distribution, overlapping the probabilities corresponding to all sky conditions. The other factor that reduces the Q_p range is the averaging of the instantaneous PAR values, in order to obtain hourly values. When an average of instantaneous values is taken, the natural fluctuations of the radiation are smoothed. In this way, the enhancement produced by the multiple reflections on the clouds is less appreciable in the hourly distributions than in the instantaneous value distributions, as showed Suehrcke et al. (1988) and Tovar et al. (1998) for broadband global irradiance. The decrease in the probability density for the principal maximum implies an

Fig. 2. Probability density distributions of global PAR for several optical air mass values. Intervals are of $40\,\mu E\,m^{-2}\,s^{-1}$ width

increment in the probability of low Q_p values, which leads to the enhancement of the second maximum. The increment in the probability of low Q_p when the optical air mass tends to higher values can also be associated with the fact that, for small zenith angles, the clouds shade on the earth surface have a smaller area than for larger angles. The horizontal layer of clouds produces an effective thickness larger for high zenith angles. Thus, for high values of the optical air mass, the effect of the clouds is stronger.

To sum up, the experimental distributions of Q_p can be modelled based on the sum of two functions:

$$f(Q_p|m_a) = f_1(Q_p) + f_2(Q_p), \qquad (5)$$

subject to the normalization condition:

$$\int_0^{Q_{p\max}} f(Q_p|m_a)dQ_p = 1. \qquad (6)$$

For functions f_1 and f_2, we have assumed a dependence on Q_p based on the Boltzmann statistic, that read as follows:

$$f_i(Q_p) = A_i \frac{\lambda_i e^{(Q_p - Q_{p0i})\lambda_i}}{[1 + e^{(Q_p - Q_{p0i})\lambda_i}]^2}, \quad i = 1, 2. \qquad (7)$$

This function yields unimodal curves, symmetrical around Q_{p0i}, where the function obtains its maximum. The parameter A_i determines the function height and λ_i is related to the width of $f_i(Q_p)$. The function has the advantage of being analytically integrable:

$$F_i(Q_p) = A_i \left[1 - \frac{1}{1 + e^{(Q_p - Q_{p0i})\lambda_i}} \right], \qquad (8)$$

and its primitive can analytically be inverted:

$$Q_p = Q_{p0i} + \frac{1}{\lambda_i} \ln \frac{F_i(Q_p)}{A_i - F_i(Q_p)}. \qquad (9)$$

These characteristics simplify the generation of synthetic data.

The coefficients A_1 and A_2 must satisfy the normalization condition:

$$\int_0^{Q_{p\max}} f(Q_p)dQ_p = A_1 \int_0^{Q_{p\max}} \frac{\lambda_1 e^{(Q_p - Q_{p01})\lambda_1}}{[1 + e^{(Q_p - Q_{p01})\lambda_1}]^2}dQ_p$$
$$+ A_2 \int_0^{Q_{p\max}} \frac{\lambda_2 e^{(Q_p - Q_{p02})\lambda_2}}{[1 + e^{(Q_p - Q_{p02})\lambda_2}]^2}dQ_p = 1. \qquad (10)$$

We obtained the parameters listed in Table 3, when fitting the various density distributions corresponding to each optical air mass value. The parameters are dependent on the optical air mass. Modelling this dependence, we have found for the distribution maxima Q_{p01} and Q_{p02} the following polynomial expressions:

$$Q_{p01} = 2882.2 - 1495.9m_a + 228.7m_a^2,$$
$$R^2 = 0.999, \qquad (11)$$

$$Q_{p02} = 2285.7 - 1433.1m_a + 241.6m_a^2,$$
$$R^2 = 0.996, \qquad (12)$$

where R^2 stand for the correlation coefficient associated with the polynomial fit used.

The principal maximum position, Q_{p01}, shifts toward lower values as the optical air mass increases. The same trend occurs for the Q_{p02} value, corresponding to the second maximum of the distribution. However, the shift is smaller than that associated with the principal maximum Q_{p01}, as can be seen by comparing the coefficients of the optical air mass term in each equation. This implies that, when the optical air mass increases, the two maxima tend to be closer.

The values of the width parameters, λ_1 and λ_2, can also be expressed in terms of the optical air mass:

$$\lambda_1 = 0.00649 + 0.0044m_a + 0.0000829m_a^2,$$
$$R^2 = 0.964, \qquad (13)$$

Table 3. Values of the parameters obtained in the adjustment of the Boltzmann's functions

Optical mass	Q_{p01} (μE m^{-2} s^{-1})	Q_{p02} (μE m^{-2} s^{-1})	λ_1	λ_2	A_1	A_2
$m_a = 1.0$	1621.5	1203.3	0.0114	0.0044	68.78	31.22
$m_a = 1.5$	1141.8	768.0	0.0126	0.0055	67.85	32.15
$m_a = 2.0$	798.6	467.1	0.0149	0.0075	66.97	33.03
$m_a = 2.5$	591.3	350.3	0.0196	0.0092	65.8	34.2
$m_a = 3.0$	443.9	245.7	0.0198	0.0131	62.26	37.74
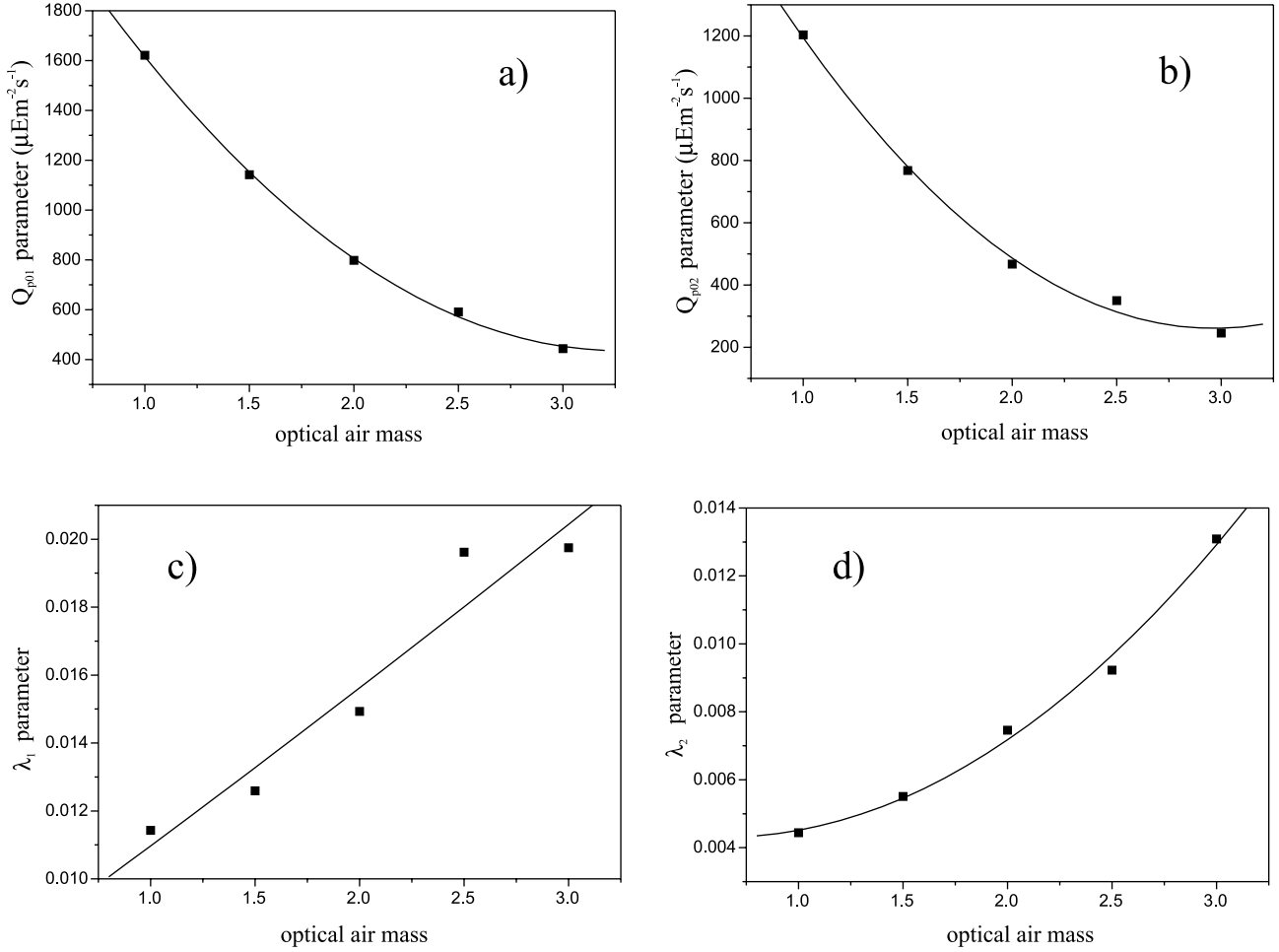
Fig. 3. Dependence on the optical air mass of the parameters of the Boltzmann's functions used to modelling the density distributions of PAR radiation values. **a)** Q_{p01} parameter; **b)** Q_{p02} parameter; **c)** λ_1 parameter; **d)** λ_2 parameter

$$\lambda_2 = 0.00494 - 0.00197 m_a + 0.00154 m_a^2,$$
$$R^2 = 0.993. \quad (14)$$

The coefficient A_1 has been fitted using the following expression:

$$A_1 = 66.86 + 3.281 m_a - 1.575 m_a^2,$$
$$R^2 = 0.975. \quad (15)$$

Considering that the parameters A_1 and A_2 dependence are constrained by the normalization condition (10), it is obvious that while A_1 decreases when the air mass increases, A_2 shows the opposite behavior. Figure 3 shows the dependence of the parameters Q_{p01}, Q_{p02}, λ_1 and λ_2, according to Eqs. (11–14). The maximum value of the distribution tends to decrease when the optical mass increases (Fig. 3a and 3b). Given an optical mass value, the maximum value of

Q_{p02} is lower than the maximum value of Q_{p01}. Additionally, the decrease rate of Q_{p02} is also lower than the decrease rate of Q_{p01}. This leads, when optical mass increases, to a decrement of the bimodal character of the distribution due to overlapping. As a consequence, given a high value of the optical mass, it becomes difficult to separate, from a statistical point of view, which PAR values correspond to clear skies having high optical mass and which correspond to cloudy skies or skies having high atmospheric turbidity. Note that Q_{p01} and Q_{p02} values decreases at a higher rate when optical mass is low and tend to stable values (around $400 \, \mu E \, m^{-2} \, s^{-1}$ for Q_{p01} and $250 \, \mu E \, m^{-2} \, s^{-1}$ for Q_{p02}) when the optical mass is high.

Figure 3c and 3d show that λ_1 and λ_2 values, and then the width of the distribution, increase
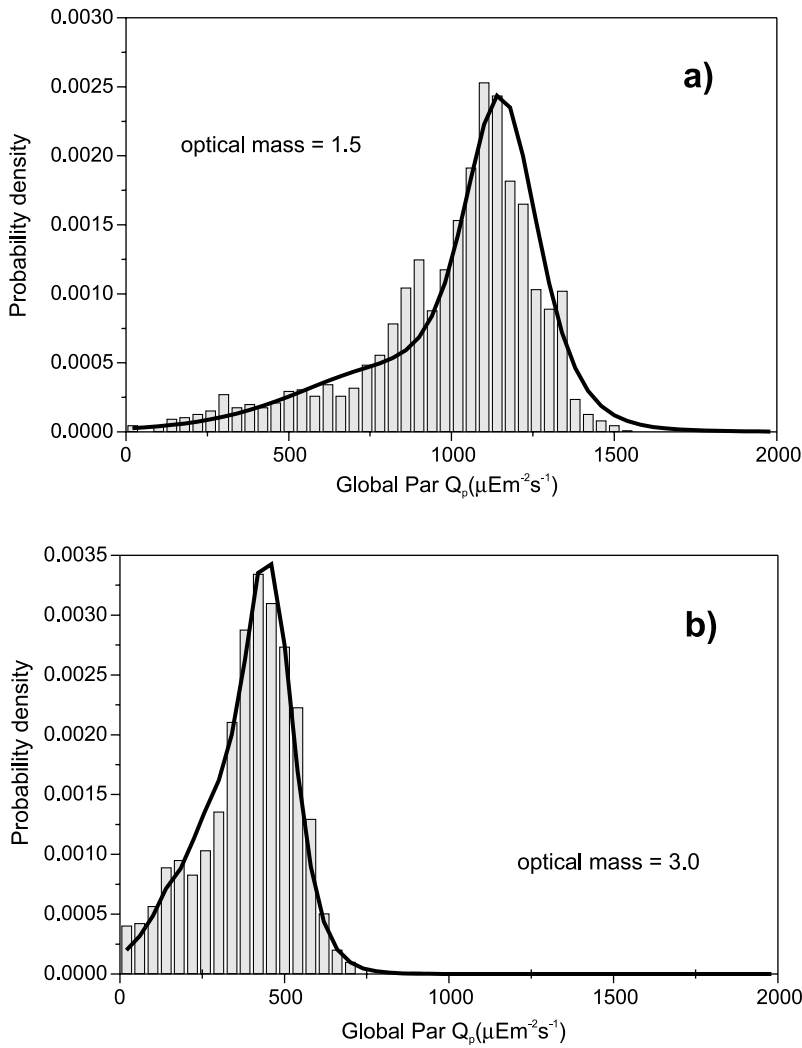
Fig. 4. Experimental data along with the proposed Boltzmann's functions. The plotted values correspond to the data set reserved for testing purposes. **a)** For optical mass $= 1.5$; **b)** for optical mass $= 3.0$

when the optical mass increases. This result makes sense, given the overlapping observed between the two functions that describe each distribution.

When the optical mass increases, the maximum values of the distributions tend to have closer values and the width of the distributions increases. This leads to an overlapping of the functions and reinforces the fact that the probability of a particular type of sky cannot be discerned from a statistical point of view.

Figure 4 shows, for values $m_a = 1.5$ and $m_a = 3.0$ of the optical mass, the proposed functions and the experimental distributions derived from the data set reserved for testing purposes. The correlation (R^2) between the experimental values and the model is close to 0.98, for both optical mass values. Similar results are obtained for other optical air mass.

4. Conclusions

A study on the frequency distribution of the PAR values has been carried out. The analysis includes the study of the dependence of PAR on the optical mass. Hourly data collected along 9 years in Southern Spain have been used.

Results shows that, for a given value of the optical mass, the density distributions are not symmetrical and have a certain degree of bimodality. The shape of the distributions shows a lower probability of having low rather than high PAR values. Additionally, two clear zones in the distributions can be delimited: the first one centred around the maximum value, the other one centred to the left of the maximum value and corresponding to the lower PAR values. The increase in the optical mass value has two effects on the PAR distributions, the first one is a

shift toward lower values of the maximum, the second one is a decrease in the range of PAR values.

The experimental distributions have been modeled using the sum of two functions based on Boltzmann's statistic. These functions are symmetrical and have adjustable parameters that present a functional dependence on the optical mass. The proposed functions provide a very good agreement between experimental and modelled values; correlation values close to 0.98 are found at optical mass values 1.5 and 3. Furthermore, the proposed functions have the advantage of being analytically integrable and that theirs derivatives can analytically be inverted. These characteristics allow the generation of synthetic data in a simple way, to be used as input for biological models and other models that includes PAR radiation as an input.

The coefficients in the equations 11 to 15, with relate Q_{p0i}, A_i and λ_i ($i = 1, 2$) to the optical mass, have been obtained based on times series collected at two Mediterranean climate locations. Therefore, these coefficients have a local character and can be different in other places having a different climate. We regard it as important to test the model in other places in order to study its dependence on local climate.

References

Aguiar R, Collares-Pereira M (1992) Statistical properties of hourly global radiation. Sol Energy 48: 157–167

Alados I, Foyo-Moreno I, Alados–Arboledas, L (1996) Photosynthetically active radiation: Measurements and modelling. Agric Forest Meteorol 78: 121–131

Bendt M, Collares-Pereira M, Rabl A (1981) The frequency distribution of daily insolation values. Sol Energy 27: 1–5

Feuillard T, Abillon JM (1989) The probability density function $P(k_h, \bar{k}_h)$ of the clearness index. A new approach. Sol Energy 43: 363–371

Gansler RA, Klein SA, Beckman WA (1995) Investigation of minute solar radiation data. Sol Energy 55: 21–27

Gordon JM, Reddy TA (1989) Stationary statistics and sequential properties of normal beam and global solar radiation on tilted surfaces. Sol Energy 42: 35–44

Iqbal M (1983) An introduction to solar radiation. Academic Press, 390 pp

Jurado M, Caridad JM, Ruiz V (1995) Statistical distribution of the clearness index with radiation data integrated over five minute intervals. Sol Energy 55: 469–473

Kasten F (1966) A new table and approximate formula for relative optical air mass. Arch Meteorol Geoph Biokl Ser B 14: 206–223

Mottus M, Ross J, Sulev M (2001) Experimental study of ratio of PAR to direct integral solar radiation under cloudless conditions. Agric Forest Meteorol 109: 161–170

Olseth JA, Skartveit A (1993) Characteristics of hourly global irradiance modelled from cloud data. Sol Energy 3: 197–204

Papaioannou G, Papanikolau N, Retails D (1993) Relationships of photosynthetically active radiation and shortwave irradiance. Theor Appl Climatol 48: 23–27

Ross J, Sulev M, Saarelaid P (1998) Statistical treatment of the PAR variability and its application to willow coppice. Agric Forest Meteorol 91: 1–21

Skartveit A, Olseth JA (1992) The probability density and autocorrelation of short-term global and beam irradiance. Sol Energy 49: 477–487

Stinger CJ, Musabilha MM (1982) The conservative ratio of photosynthetically active to total radiation in the tropics. J Appl Ecol 19: 853–858

Suehrcke H, McCormick PG (1988). The frequency distribution of instantaneous insolation values. Sol Energy 40: 413–422

Tovar J, Olmo FJ, Alados-Arboledas L (1998) One-minute global irradiance probability density distributions conditioned to the optical air mass. Sol Energy 62: 387–393

Yocum CS, Allen LH, Lemon ER (1969) Photosynthesis under field conditions, VI. Solar radiation balance and photosynthetic efficiency. Agron J 56: 249–253

Authors' addresses: Joaquín Tovar-Pescador (e-mail: jtovar@ujaen.es), D. Pozo-Vazquez, Departamento de Física, Escuela Politécnica Superior, Universidad de Jaén, 23071 Jaén, Spain; J. Batlles, G. López, Department of Applied Physics, University of Almería, Spain; D. Muñoz-Vicente, Department of Computer Sciences, University of Jaén, Spain.